

Pressure induced superconductivity bordering a charge-density-wave state in NbTe₄ with strong spin-orbit coupling

Xiaojun Yang^{1,2}, Yonghui Zhou³, Mengmeng Wang¹, Hua Bai¹, Xuliang Chen³,
Chao An³, Ying Zhou³, Qian Chen¹, Yupeng Li¹, Zhen Wang¹, Jian Chen¹,
Chao Cao⁴, Yuke Li⁴, Yi Zhou^{1,6}, Zhaorong Yang^{3*} and Zhu-An Xu^{1,5,6†}

¹ *State Key Laboratory of Silicon Materials and Department of Physics,
Zhejiang University, Hangzhou 310027, China.*

² *School of Physics and Optoelectronics,
Xiangtan University, Xiangtan 411105, China*

³ *Anhui Province Key Laboratory of Condensed Matter Physics at Extreme Conditions,
High Magnetic Field Laboratory, Chinese Academy of Science, Hefei 230031, China*

⁴ *Department of Physics, Hangzhou Normal University, Hangzhou 310036, China*

⁵ *Zhejiang California International NanoSystems Institute,
Zhejiang University, Hangzhou 310058, China*

⁶ *Collaborative Innovation Centre of Advanced
Microstructures, Nanjing 210093, P. R. China*

(Dated: April 23, 2018)

* Electronic address: zryang@issp.ac.cn

† Electronic address: zhuan@zju.edu.cn

Transition-metal chalcogenides host various phases of matter, such as charge-density wave (CDW), superconductors, and topological insulators or semimetals. Superconductivity and its competition with CDW in low-dimensional compounds have attracted much interest and stimulated considerable research. Here we report pressure induced superconductivity in a strong spin-orbit (SO) coupled quasi-one-dimensional (1D) transition-metal chalcogenide NbTe₄, which is a CDW material under ambient pressure. With increasing pressure, the CDW transition temperature is gradually suppressed, and superconducting transition, which is fingerprinted by a steep resistivity drop, emerges at pressures above 12.4 GPa. Under pressure $p = 69$ GPa, zero resistance is detected with a transition temperature $T_c = 2.2$ K and an upper critical field $\mu_0 H_{c2} = 2$ T. We also find large magnetoresistance (MR) up to 102% at low temperatures, which is a distinct feature differentiating NbTe₄ from other conventional CDW materials.

Introduction

Transition-metal chalcogenides possess rich structural chemistry and a wide variety of unusual physical properties[1–3]. The latter includes, for instance, charge density wave (CDW)[3], superconductivity[4–7] and recently reported extremely large magnetoresistance in WTe₂[8–13]. Among chalcogenides, tellurides are usually different from sulfides and selenides in crystal structures, electronic structures and physical properties, due to the diffusive nature of the tellurium valence orbitals[14] and thus more covalent character of tellurium[1]. While sulfides and selenides, such as NbS₂, NbSe₂ and NbSe₃, were intensively studied in the context of CDW and/or superconductivity[3, 4, 15], tellurides have not received much attention until recently[8–13]. One important feature of tellurides is that the atomic number of Te is very large, resulting in a strong spin-orbital (SO) coupling. Nowadays, topological materials with strong SO coupling have been drawing plenty of attention in condensed matter physics[16]. It is highly desirable to discover novel superconductors with strong SO coupling for understanding the nature of topological superconductivity. On the other hand, low dimensionality is accompanied by strong lattice instability. Additional interest for pursuing a quasi-1D material with itinerant electrons comes from the possible realization of Luttinger

liquid, in which an exotic spin-charge separation is expected[17]. Thus, it should be of great interest to study superconductivity in quasi-1D tellurides with large atomic number[14, 18], where competing interactions might give rise to interacting ground states.

The magnetoresistance (MR) in ordinary non-magnetic metals is a relatively weak effect and usually at the level of a few percent[19, 20]. Materials exhibiting large MR are not only utilized to enlarge the sensitivity of read/write heads of magnetic storage devices, e.g., magnetic memory[21] and hard drives[22], but also stimulating many fundamental researches[8, 23]. Typically, large negative MR occurs in thin-film metals [24], manganese based perovskites[25, 26] and some disordered systems[27, 28], while large positive MR has been observed in semiconductors[29] and semimetals[8, 30]. In general, there exists only a few of CDW materials, which show large positive MR[31–33]. The origin of the huge positive MR effect in the CDW state is still under debate. Exploring more CDW materials with large MR may help to clarify the controversial explanations.

NbTe₄ and TaTe₄ belong to the same group of quasi-1D CDW materials (space group P4/mcc). The structure of NbTe₄ was first determined by Selte and Kjekshus in 1964[34]. The metal atoms Nb form linear chains along the tetragonal *c*-axis and the Te atoms form square antiprismatic formulae in which the metal atoms confined (Fig. 1(a,b)). Superlattice reflections indicate that the *a*-axis is doubled and the *c*-axis is tripled, leading to an enlarged unit cell $2a^* \times 2a^* \times 3c^*$ [34, 35]. NbTe₄ undergoes a strong lattice distortion around room temperature to form an incommensurate charge density wave (CDW) phase[35–37]. The resulting CDW superstructure in NbTe₄ was visualized by scanning tunneling microscopy (STM)[37]. Intriguingly, the CDW ordering in NbTe₄ is highly anisotropic due to the quasi-1D chain structure. Strikingly, there exist three CDW orders in NbTe₄, two are incommensurate with wave vectors $\vec{q}_1 = (0, 0, 0.311c^*)$ and $\vec{q}_2 = (0.5a^*, 0.5b^*, 0.344c^*)$, respectively, and the third is commensurate with $\vec{q}_3 = (0.5a^*, 0, \frac{1}{3}c^*)$ [35]. The crystal structure of NbTe₄ is depicted in Fig. 1(a, b). The displacements of Nb ion in a single column for the commensurate phase are shown in Fig. 1c, which can also be found in previous literature[38]. Indeed, NbTe₄ and TaTe₄ are the only two reported crystals in which three CDWs coexist [35]. In this paper, we report large magneto-resistance and high pressure induced superconductivity in NbTe₄. The CDW transition temperature is strongly suppressed by applied pressure, and superconductivity fingerprint of steep resistivity drop emerges when pressure exceeds 12.4 GPa. Under pressure $p = 69$ GPa, zero resistance is

reached with a transition temperature $T_c = 2.2$ K and an upper critical field of 2 T. We also observed large magnetoresistance (MR) up to 102% at low temperatures in NbTe₄, which is rarely observed in conventional CDW systems.

Results and Discussions

Figure 1d displays the X-ray diffraction pattern of NbTe₄ single crystal. Only multiple reflections of the (0 *l* 0) planes can be detected, consistent with the quasi-one-dimensional crystal structure depicted in Fig. 1(a, b). The interplane spacing is determined to be 6.499 Å, agreeing with the previous reported value of the NbTe₄ phase [34]. For the (030) peak, the full width at half-maximum is only 0.03°, indicating high quality of the crystals.

The temperature dependence of resistivity under various applied magnetic fields ($\mu_0 H$ up to 15 T) is summarized in Fig. 2a. In zero field, the room temperature resistivity is 59.2 $\mu\Omega\cdot\text{cm}$ and decreases to 9.4 $\mu\Omega\cdot\text{cm}$ at $T = 2$ K, yielding a residual resistivity ratio (RRR) of 6.3. Low RRR in NbTe₄ single crystals has been commonly reported, which is irrespective of growth conditions [39, 40]. To understand the origin of the poor RRR, we performed the measurements of energy dispersive X-ray spectroscopy (EDXS). The chemical composition determined by EDXS gives the atomic ratio Nb:Te = 0.8:4, with a measurement error of $\pm 3.5\%$ depending on the elements measured. This result indicates that there exists significant deficiency for Nb, which may be responsible for the poor RRR. To get further insight into the resistivity data, we take the partial derivative of resistivity with respect to temperature, as shown in the inset of Fig. 2a. At $T^* = 200$ K a cusp is observed, consistent with the previous reports[39, 40]. It is known that the two incommensurate superlattices with $\vec{q}_1 = (0, 0, 0.311c^*)$ and $\vec{q}_2 = (0.5a^*, 0.5b^*, 0.344c^*)$ are stable at room temperature in NbTe₄. Below room temperature, additional superlattice ordering with $\vec{q}_3 = (0.5a^*, 0, \frac{1}{3}c^*)$ emerges at about 200 K. The change of the slope in the temperature dependence of resistivity at 200 K should be due to the appearance of the \vec{q}_3 superlattice[39, 40]. Usually, more drastic anomalies in resistivity should be observed at the CDW transition temperatures. For example, two sharp increases in resistivity were observed in NbSe₃ at 145 and 59 K [15], corresponding to about 20% and 48% of conduction electrons condensating into the CDW states, respectively[15, 33]. The observed small change of resistivity around 200 K in NbTe₄ is indicative of a finite but slight decrease of free carrier density associated

with the reconstruction of the Fermi surface by Brillouin zone refolding. The anomaly at around $T_L = 50$ K may be due to the lock-in transition into the $2a^* \times 2a^* \times 3c^*$ superstructure, which is worthy of further clarification[40]. The anomalies at $T^* = 200$ K and $T_L = 50$ K, which were also observed in previous reports[39, 40], further confirm the CDW features observed in NbTe₄.

The field ($H//b$) dependence of resistance ($I//c$) at various temperatures is shown in Fig. 2b. The magneto-resistance (MR), which is defined as $MR = [\rho(15T) - \rho(0)]/\rho(0)$, rises up to 102% under a magnetic field of 15 T at $T = 2$ K. Although the MR value of NbTe₄ is orders of magnitude smaller than that of WTe₂[8] and Bi[30], it is much larger than that of a usual single-band weakly interacting electron system, in which the MR is usually at the level of a few percent[8, 20]. For a single-band noninteracting electron system, the Hall field exactly balances the Lorentz force, and the electron moves as if in zero field without being deflected; thus, there is no remarkable magnetoresistance[20, 41].

Figure 3 displays the field ($H//b$) dependence of Hall resistivity ($I//c$) ρ_{yx} at various temperatures. At 2 K, ρ_{yx} is positive under low fields but switches to negative sign in higher fields. With increasing temperature, the required field where ρ_{yx} changes its sign decreases. The curvature and sign reversal in the Hall resistivity indicate the coexistence of hole-type minority carriers with high mobility and electron-type majority carriers with low mobility[42, 43]. The multiband nature of NbTe₄ is also manifested in the breakdown of the Kohler's rule, as plotted in the inset of Fig. 3. According to the Kohler's rule, if only one relaxation time τ exists in metals, then MR can be characterized by a function of $\mu_0 H/\rho(0)$, and the results for different temperatures should collapse into a single curve[41, 44]. As shown clearly in the inset of Fig. 3, the Kohler's rule is violated in NbTe₄, as evident by the non-overlapping of the MR curves at different temperatures. The observation indicates more than one relaxation time τ exist, supporting the multiband result obtained by the Hall measurements.

Materials exhibiting a large magneto-resistance have potential device applications and thus have been attracting researchers' interest [45]. The most well-known examples are the giant magnetoresistance in magnetic multilayers[24] and colossal magnetoresistance in manganites[26], both of them rely on the coupling between spin configuration and charge transport. However, even among nonmagnetic materials, extremely large magnetoresistance (MR) may arise in semimetals with electron-hole Fermi surface (FS) compensation[46–49].

As a discussion of the multiband effects in NbTe₄, we define the direction of the current (Hall voltage) as the x -axis (y -axis). Even though no net current should exist in the y -direction, the currents in the y -direction by one particular type of carriers may be non-zero in a multiband system. When we applied magnetic field, the y -direction currents should be affected by the Lorentz force which is antiparallel to the x -direction[50]. The back flow of carriers provides a substantial source of the large magnetoresistance in metals with multiple bands like MgB₂[41] and semimetals like Bi[48] and WTe₂[8]. Owing to the coexistence of both electron- and hole-type carriers, the large MR in NbTe₄ may be attributed to multiband effects. We employed a two band mode to fit the ρ_{xx} and ρ_{yx} data simultaneously in the low field region[51]. The values of n_e and n_h are close to each other at all the measured temperatures, which suggests that the large MR should result from the electron-hole compensation effect. The mobilities μ_e and μ_h increase with decreasing temperatures as the usual metals. Meanwhile, the carrier concentrations decrease significantly at low temperatures, which occurs commonly in a CDW system. At $T = 2$ K, μ_e is $0.22 \text{ m}^2\text{V}^{-1}\text{s}^{-1}$, while μ_h is $0.29 \text{ m}^2\text{V}^{-1}\text{s}^{-1}$. Actually large magnetoresistance was also observed in the CDW materials NbSe₃[31, 33] and AMo₆O₁₇ (A = Na, K, and Tl)[32]. It has been proposed that the large MR in these CDW systems may result from the magnetic-field-induced enhancement of the CDW gap[31], but a study by Tritt et al.[52] presented negative results on such a claim. Until now, the nature of the huge positive MR effect in the CDW state is still ambiguous. Actually, only a few CDW materials show large positive MR[31–33]. The origin of the large MR in NbTe₄ deserves further investigation.

Superconductivity often occurs in the proximity of other competing ordered states. Both high- T_c cuprates and Fe-based superconductors are close to antiferromagnetic (AFM) ordered states[53, 54]. The AFM order in Fe-based superconductor is of a spin density wave (SDW)-type. For CDW materials, high pressure or chemical doping can continuously suppress the CDW order, and then superconducting transition temperature is enhanced or superconducting state emerges after the suppression of CDW state[55, 56]. The weakening of competing orders normally favors superconductivity[57]. The CDW order of NbTe₄ survives up to very high temperatures. Thus it is interesting to investigate whether superconductivity can be induced by pressure.

Figure 4a shows the evolution of resistance ($I//c$) as a function of temperature of the NbTe₄ single crystal at various pressures from 5 GPa to 69 GPa. The samples used in high

pressure and ambient pressure measurements are two different ones, but they are from the same batch. Under an applied pressure of $p = 5$ GPa, the cusp associated with the appearance of the \vec{q}_3 -superlattice CDW transition is suppressed to $T^* = 173$ K, as shown in Fig. 4b. The MR decreases to less than 10% with an applied pressure of 5 GPa, and becomes smaller and smaller with an increasing pressure, as shown in Fig. 4c. When the pressure increases up to 12.4 GPa, the cusp associated with the CDW transition is suppressed and becomes too weak to be distinguished in the resistivity curve, instead, a sudden resistivity decrease presents at $T \sim 2.4$ K, which could be a fingerprint of superconductivity. So we keep increasing the pressure to trace the superconducting transition. Upon further increasing pressure, at $T = 1.7$ K, which is the base temperature of our high pressure measurement system, the resistance drops to very small. Finally, under $p = 69$ GPa, which is the highest pressure we can apply, zero resistance has been detected. The low-T resistance appears to increase monotonically with pressure. In contrast, the room-temperature resistance keeps increasing up to 12.4 GPa, and then steadily decreases, which coincides with the disappearance of the CDW phase. Whether the variation in room-temperature resistance is correlated with the CDW order deserves further clarification. T_c around 2.2 K is stabilized for the pressure range from 10 to 69 GPa. Such a wide stabilization pressure range could be a result of heavy doping due to Nb deficiency up to 0.2. Fig. 4d shows the suppression of superconductivity under magnetic fields ($H//b$). The inset gives the temperature dependence of the upper critical field $\mu_0 H_{c2}(T)$, determined by using 90% normal state resistivity criterion. The temperature dependence of $\mu_0 H_{c2}(T)$ is nearly linear in the investigated temperature range. According to the Ginzburg-Landau theory, the upper critical field H_{c2} evolves with temperature following the formula $H_{c2}(T) = H_{c2}(0)(1 - t^2)/(1 + t^2)$, where t is the renormalized temperature T/T_c . It is found that the experimental upper critical field $\mu_0 H_{c2}(T)$ can be well fitted by this model and its zero-temperature limit is extracted to be 2.0 T. Due to the limited temperature range, the estimated $\mu_0 H_{c2}(0)$ by this way may be of considerable error.

The temperature-pressure phase diagram is summarized in Fig. 5. The CDW transition temperature in NbTe₄ is strongly suppressed with an applied high pressure. Accompanying the suppression of the CDW order, superconductivity fingerprint appears. Such superconducting phase diagrams, where superconductivity may compete with different kind of orders, have been observed in many systems, including high- T_c cuprates, Fe-based superconductors,

NbSe₂ and Cu_xTiSe₂[53–56]. Barath *et al.* proposed that the superconducting pairing mechanism in Cu_xTiSe₂ could be associated with the quantum criticality, stemming from the fluctuations of CDW order[58]. There are also many theoretical works on the superconducting dome in transition metal dichalcogenides (TMDCs), and pursuing the nature of the observed superconducting states is still on-going[59, 60]. High temperature high pressure treatment could induce phase transformation in NbTe₄[61], which may be relevant to the occurrence of superconductivity. Further investigation on this issue is of potential interest. Since the physical properties of NbTe₄ and TaTe₄ show numerous similar features, the further research on pressure effect of TaTe₄ should be gainful[62]. As a low dimensional chalcogenide, it could be fascinating to explore whether intercalation or doping could induce superconductivity, or at least decrease the critical superconducting pressure, as the case in Cu_xTiSe₂[58], Cu_xBi₂Se₃[63], Ir_{1-x}Pd_xTe₂[16], (NbSe₄)_{3.33}I[64]. Primarily because of the strong SO coupling, the appealing Majorana surface state has been suggested to exist in Cu_xBi₂Se₃ superconductor [63, 65]. Due to the large atom number in NbTe₄, it is expected to own strong SO coupling. Furthermore, a recent theoretical work has proposed monolayer hole-doped TMDCs as candidates for topological superconductors[66], which makes transition metal chalcogenide systems more fascinating. Thus it becomes quite interesting to explore the possible presence of nonconventional quantum states in NbTe₄. Our work may provide another promising system for exploring novel topological superconductors.

Summary

In conclusion, we discovered unusually large magnetoresistance(MR) and pressure induced superconductivity with a maximum T_c of 2.2 K in a quasi-one-dimensional (1D) transition-metal chalcogenide NbTe₄ with strong spin-orbit coupling. Superconductivity appears when the CDW order is suppressed by high pressure. Although T_c is relatively low, the large MR and strong SO coupling make NbTe₄ a promising candidate for the exploration of novel superconductors.

Methods

Sample synthesis and characterization

The NbTe₄ crystals were grown by a self-flux method. Powders of the elements Nb (99.97%) and Te (99.99%), all from Alfa Aesar, in an atomic ratio of Nb:Te = 1:8 were thoroughly mixed together, loaded, and sealed into an evacuated quartz ampule. The ampule was slowly heated up to 1273 K and held for 25 h. After that, it was slowly cooled to 873 K at a rate of 3 K/h, followed by furnace cooling down to room temperature. Shiny, gray-black soft crystals in flattened needle shapes were harvested with a typical dimension of $1.2 \times 0.02 \times 0.02$ mm³, as shown in Fig. 1(e). Single crystal X-ray diffraction (XRD) was performed at room temperature using a PANalytical X-ray diffractometer (Model EMPYREAN) with a monochromatic CuK_{α1} radiation. Energy-dispersive x-ray spectroscopy (EDXS) was collected by an Octane Plus Detector (AMETEX EDAX), equipped in a field-emitting scanning electron microscope (SEM, Hitachi S-4800).

Measurements

The resistance data was collected using standard four-probe method in a screw-pressure-type diamond anvil cell (DAC), which is made of non-magnetic Cu-Be alloy. The diamond culet was about 320 μm in diameter. A T301 stainless steel gasket was pre-indented from a thickness of 220 μm to 35 μm, leaving a pit inside the gasket. A hole with diameter of 300 μm was drilled in the center of the pit by laser ablation. The pit of the indented gasket was then covered with a mixture of epoxy and fine cubic boron nitride (cBN) powder and compressed tightly to insulate the electrode leads from the metallic gasket. Next, the cBN-covered pit served as the sample chamber, where a NbTe₄ single crystal in dimension of 200 μm × 35 μm × 5 μm was inserted without the pressure-transmitting medium, together with a ruby ball served as a pressure marker at the top of the sample. The value of the pressure was determined by the ruby fluorescence method. Platinum (Pt) foil with a thickness of 5 μm was used as electrodes. The gasket surface outside the pit was insulated from the electrode leads by a layer of Scotch tape. The DAC was put inside a home-made multifunctional measurement system (1.8-300 K, JANIS Research Company Inc.; 0-9 T, Cryomagnetics Inc.) with helium (He) as the medium for heat conduction to obtain high efficiency of heat transfer and good precision of temperature control. Two Cernox resistors (CX-1050-CU-HT-1.4 L) located near the DAC were employed to ensure the accuracy of temperature in the presence of magnetic field. The ambient-pressure electrical transport measurements were carried out in a Oxford cryostat system with magnetic field up to 15 T and temperature

down to 1.5 K. Ohmic contacts were made with gold wires and silver paste.

- [1] Mar, A., Jobic, S. & Ibers, J. A. Metal-Metal vs Tellurium-Tellurium Bonding in WTe_2 and Its Ternary Variants TaIrTe_4 and NbIrTe_4 . *J. Am. Chem. Soc.* **114**, 8963-8971 (1992).
- [2] Monceau, P. Electronic crystals: an experimental overview. *Adv. Phys.* **61**, 325-581 (2012).
- [3] Moncton, D. E., Axe, J. D. & DiSalvo, F. J. Neutron scattering study of the charge-density wave transitions in 2H-TaSe_2 and 2H-NbSe_2 . *Phys. Rev. B* **16**, 801-819 (1977).
- [4] Morris, R. C., Coleman, R. V. & Bhandari, R. Superconductivity and magnetoresistance in NbSe_2 . *Phys. Rev. B* **5**, 895-901 (1972).
- [5] Gamble, F. R. *et al.* Superconductivity in Layered Structure Organometallic Crystals. *Science* **168**, 568-570, (1970).
- [6] Pan, X. C. *et al.* Pressure-driven dome-shaped superconductivity and electronic structural evolution in tungsten ditelluride. *Nat. Commun.* **6**, 7805 (2015).
- [7] Kang, D. *et al.* Superconductivity emerging from a suppressed large magnetoresistant state in tungsten ditelluride. *Nat. Commun.* **6**, 7804 (2015).
- [8] Ali, M. N. *et al.* Large, non-saturating magnetoresistance in WTe_2 . *Nature* **514**, 205-208 (2014).
- [9] Cai, P. L. *et al.* Drastic pressure effect on the extremely large magnetoresistance in WTe_2 : quantum oscillation study. *Phys. Rev. Lett.* **115**, 057202 (2015).
- [10] Zhu, Z. *et al.* Quantum Oscillations, Thermoelectric Coefficients, and the Fermi Surface of Semimetallic WTe_2 . *Phys. Rev. Lett.* **114**, 176601 (2015).
- [11] Jiang, J. *et al.* Signature of Strong Spin-Orbital Coupling in the Large Nonsaturating Magnetoresistance Material WTe_2 . *Phys. Rev. Lett.* **115**, 166601 (2015).
- [12] Zhao, Y. *et al.* Anisotropic magnetotransport and exotic longitudinal linear magnetoresistance in WTe_2 crystals. *Phys. Rev. B* **92**, 041104(R) (2015).
- [13] Pletikosić, I. *et al.* Electronic Structure Basis for the Extraordinary Magnetoresistance in WTe_2 . *Phys. Rev. Lett.* **113**, 216601 (2014).
- [14] Jiao, W. H. *et al.* Superconductivity in a Layered $\text{Ta}_4\text{Pd}_3\text{Te}_{16}$ with PdTe_2 Chains. *J. Am. Chem. Soc.* **136**, 1284-1287 (2014).
- [15] Ong, N. P. & Monceau, P. Anomalous transport properties of a linear-chain metal: NbSe_3 .

- Phys. Rev. B* **16**, 3443-3455 (1977).
- [16] Yang, J. J. *et al.* Charge-Orbital Density Wave and Superconductivity in the Strong Spin-Orbit Coupled IrTe₂:Pd. *Phys. Rev. Lett.* **108**, 116402 (2012).
- [17] Voit, J. One-Dimensional Fermi Liquids. *Rep. Prog. Phys.* **58**, 977 (1995).
- [18] Bao, J. K. *et al.* Superconductivity in Quasi-One-Dimensional K₂Cr₃As₃ with Significant Electron Correlations. *Phys. Rev. X* **5**, 011013 (2015).
- [19] Lin, X. *et al.* Superconductivity induced by La doping in Sr_{1-x}La_xFBiS₂. *Phys. Rev. B* **87**, 020504(R) (2013).
- [20] Pippard, A. B. *Magnetoresistance in Metals* (*Cambridge University*, Cambridge, 1989).
- [21] Moritomo, Y. *et al.* Giant magnetoresistance of manganese oxides with a layered perovskite structure. *Nature* **380**, 141-144 (1996).
- [22] Daughton, J. M. GMR applications. *J. Magn. Magn. Mater.* **192**, 334-342 (1999).
- [23] Urushibara, A. *et al.* Insulator-metal transition and giant magnetoresistance in La_{1-x}Sr_xMnO₃. *Phys. Rev. B* **51**, 14103-14109 (1995).
- [24] Egelhoff, W. F. *et al.* Magnetoresistance values exceeding 21% in symmetric spin valves. *J. Appl. Phys.* **78**, 273-277 (1995).
- [25] Ramirez, A. P., Cava, R. J. & Krajewski, J. Colossal magnetoresistance in Cr-based chalcogenide spinels. *Nature* **386**, 156-159 (1997).
- [26] Jin, S. *et al.* Colossal magnetoresistance in La-Ca-Mn-O ferromagnetic thin films. *J. Appl. Phys.* **76**, 6929-6933 (1994).
- [27] Yang, X. *et al.* Sr_{0.9}K_{0.1}Zn_{1.8}Mn_{0.2}As₂: A ferromagnetic semiconductor with colossal magnetoresistance. *EPL* **107**, 67007 (2014).
- [28] Yang, X. *et al.* K and Mn co-doped BaCd₂As₂: A hexagonal structured bulk diluted magnetic semiconductor with large magnetoresistance. *J. Appl. Phys.* **114**, 223905 (2013).
- [29] Xu, R. *et al.* Large magnetoresistance in non-magnetic silver chalcogenides. *Nature* **390**, 57-60 (1997).
- [30] Alers, P. B. & Webber, R. T. The magnetoresistance of bismuth crystals at low temperatures. *Phys. Rev.* **91**, 1060-1065 (1953).
- [31] Yasuzuka, S. *et al.* Pressure effect on large magnetoresistance in the lower charge-density-wave transition of NbSe₃. *Phys. Rev. B* **60**, 4406-4409 (1999).
- [32] Tian, M., Yue, S. & Zhang, Y. Magnetoresistance of quasi-two-dimensional purple bronzes

- AMo₆O₁₇ (A =Na, K, and Tl). *Phys. Rev. B* **65**, 104421 (2002).
- [33] Shen, J. Q. *et al.* The magnetoresistance of the quasi-one-dimensional conductor NbSe₃. *J. Phys.: Condens. Matter* **15**, 5353-5358 (2003).
- [34] Selte, K. & Kjekshus, A. On the Crystal Structure of NbTe₄. *Acta Chem. Scand.* **18**, 690-696 (1964).
- [35] Boswell, F. W., Prodan, A. & Brandon, J. K. Charge-density waves in the quasi-one-dimensional compounds NbTe₄ and TaTe₄. *J. Phys. C: Solid State Phys.* **16**, 1067-1076 (1983).
- [36] Mahy, J., Landuyt, J. V. & Amelinckx, S. Electron Diffraction Evidence for Superstructures in TaTe₄ and NbTe₄. *Phys. Status Solidi A* **77**, K1 (1983).
- [37] Prodan, A. *et al.* Scanning tunneling microscope study of charge-density-wave modulations in NbTe₄. *Phys. Rev. B* **57**, 6235-6238 (1998).
- [38] Walker, M. B. & Morelli, R. NbTe₄: A model for a class of incommensurate-to-incommensurate phase transitions. *Phys. Rev. B* **38**, 4836-4839 (1988).
- [39] Ikari, T., Berger, H. & Levy, F. Electrical Properties of NbTe₄ and TaTe₄. *Phys. Stat. Sol. (b)* **139**, K37-K40 (1987).
- [40] Tadaki, S., *et al.* Electrical properties of NbTe₄ and TaTe₄. *Synthetic Metals* **38**, 227-234 (1990).
- [41] Li, Q. *et al.* Large Anisotropic Normal-State Magnetoresistance in Clean MgB₂ Thin Films. *Phys. Rev. Lett.* **96**, 167003 (2006).
- [42] Luo, Y. *et al.* Pressure-enhanced superconductivity in Eu₃Bi₂S₄F₄. *Phys. Rev. B* **90**, 220510(R) (2014).
- [43] Wang, K. *et al.* Anisotropic giant magnetoresistance in NbSb₂. *Sci. Rep.* **4**, 7328 (2014).
- [44] Ziman, J. M. *Electrons and Phonons*, Classics Series (*Oxford University Press*, New York, 2001).
- [45] Takatsu, H. *et al.* Extremely Large Magnetoresistance in the Nonmagnetic Metal PdCoO₂. *Phys. Rev. Lett.* **111**, 056601 (2013).
- [46] Yang, F. Y. *et al.* Large Magnetoresistance of Electrodeposited Single-Crystal Bismuth Thin Films. *Science* **284**, 1335-1337 (1999).
- [47] Yang, X. *et al.* Giant linear magneto-resistance in nonmagnetic PtBi₂. *Appl. Phys. Lett.* **108**, 252401 (2016).
- [48] Du, X. *et al.* Metal-Insulator-Like Behavior in Semimetallic Bismuth and Graphite. *Phys. Rev.*

- Lett.* **94**, 166601 (2005).
- [49] Kasahara, Y. *et al.* Exotic Superconducting Properties in the Electron-Hole-Compensated Heavy-Fermion "Semimetal" URu₂Si₂. *Phys. Rev. Lett.* **99**, 116402 (2007).
- [50] Singleton, J. Band Theory and Electronic Properties of Solids. (*Oxford University Press*, 2001).
- [51] See supplementary material for a simultaneous fitting of ρ_{xx} and ρ_{yy} data by the two band semiclassical model.
- [52] Tritt, T. M. *et al.* Charge-Density-Wave Carrier Concentration in NbSe₃ as a Function of Magnetic Field and Temperature. *Phys. Rev. Lett.* **61**, 1776 (1988).
- [53] Cruz, C. *et al.* Magnetic order close to superconductivity in the iron-based layered LaO_{1-x}F_xFeAs systems. *Nature* **453**, 899-902 (2008).
- [54] Paglione, J. & Greene, R. L. High-temperature superconductivity in iron-based materials. *Nat. Phys.* **6**, 645-658 (2010).
- [55] Morosan, E. *et al.* Superconductivity in Cu_xTiSe₂. *Nat. Phys.* **2**, 544-550 (2006).
- [56] Morris, R. C. Connection between charge-density waves and superconductivity in NbSe₂. *Phys. Rev. Lett.* **34**, 1164-1166 (1975).
- [57] Regueiro, M. N., Mignot, J. M. & Castello, D. Superconductivity at High Pressure in NbSe₃. *EPL* **18**, 53-57 (1992).
- [58] Barath, H. *et al.* Quantum and Classical Mode Softening Near the Charge-Density-Wave-Superconductor Transition of Cu_xTiSe₂. *Phys. Rev. Lett.* **100**, 106402 (2008).
- [59] Das, T. & Dolui, K. Superconducting dome in MoS₂ and TiSe₂ generated by quasiparticle-phonon coupling. *Phys. Rev. B* **91**, 094510 (2015).
- [60] Rösner, M., Haas, S. & Wehling, T. O. Phase diagram of electron-doped dichalcogenides. *Phys. Rev. B* **90**, 245105 (2014).
- [61] Bjerkelund, E., Kjekshus, A. & Meisalo, V. High Pressure Induced Transformations in NbTe₄ and TaTe₄. *Acta. Chem. Scand.* **22**, 3336 (1968).
- [62] Luo, X. *et al.* Resistivity plateau and large magnetoresistance in the charge density wave system TaTe₄. *Appl. Phys. Lett.* **110**, 092401 (2017).
- [63] Hor, Y. S. *et al.* Superconductivity in Cu_xBi₂Se₃ and its Implications for Pairing in the Undoped Topological Insulator. *Phys. Rev. Lett.* **104**, 057001 (2010).
- [64] Wang, Z. Z. *et al.* Charge density transport in a novel halogened transition metal tetrachalco-

- genide $(\text{NbSe}_4)_{3.33}\text{I}$. *Solid State Commun.* **47**, 439-443 (1983).
- [65] Fu, L. & Berg, E. Odd-Parity Topological Superconductors: Theory and Application to $\text{Cu}_x\text{Bi}_2\text{Se}_3$. *Phys. Rev. Lett.* **105**, 097001 (2010).
- [66] Hsu, Y. *et al.* Topological superconductivity in monolayer transition metal dichalcogenides. *Nat. Commun.* **8**, 14985 (2017).

Acknowledgements

We thank Yi Zheng and Guanghan Cao for valuable discussions and helpful suggestions. This work is supported by the Ministry of Science and Technology of China (Grant No. 2016YFA0300402 and 2016YFA0401804), NSF of China (Contract Nos. U1332209, 11574323, and U1632275). X. C. thanks for the support from the Natural Science Foundation of Anhui Province (1708085QA19).

Author contributions

Zhu-an Xu and Xiaojun Yang designed the research. Zhu-an Xu administered the experiment. Xiaojun Yang synthesized the samples. Xiaojun Yang and Yonghui Zhou performed the measurements. Mengmeng Wang, Hua Bai, Xuliang Chen, Chao An, Ying Zhou, Qian Chen, Yupeng Li, Zhen Wang, Jian Chen, Chao Cao, Yuke Li, Yi Zhou and Zhaorong Yang presented helpful suggestions in the measurements and in the data analysis. Zhu-an Xu, Xiaojun Yang and Zhaorong Yang analyzed the data, interpreted the results, and wrote the paper.

Additional Information

Competing Interests: The authors declare no competing interests.

Correspondence and requests for materials should be addressed to Zhu-an Xu (zhuan@zju.edu.cn) and Zhaorong Yang (zryang@issp.ac.cn).

Figures:

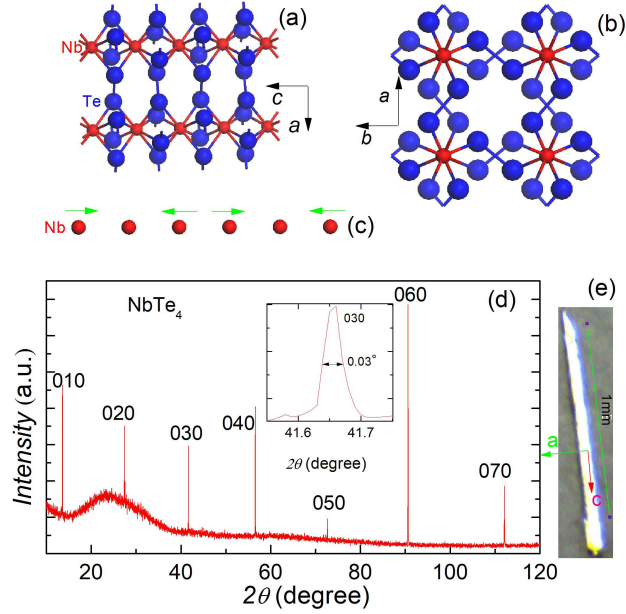


FIG. 1: **Structural characterization by x-ray diffractions for NbTe_4 .** (a,b), The basic crystal structure of NbTe_4 projected along the $[010]$ (a) and $[001]$ (b) directions. (c), The red solid circles represent equidistant Nb ions on the axis of a single column of the basic structure; the arrows show the displacements and resultant trimerizations of the Nb ions in the commensurate phase. (d), XRD structure characterization of a NbTe_4 single crystal. Only $(0\ l\ 0)$ peaks can be observed. The inset: The enlarged XRD curve of (030) peak. (e), A typical crystal of NbTe_4 , with crystallographic directions marked.

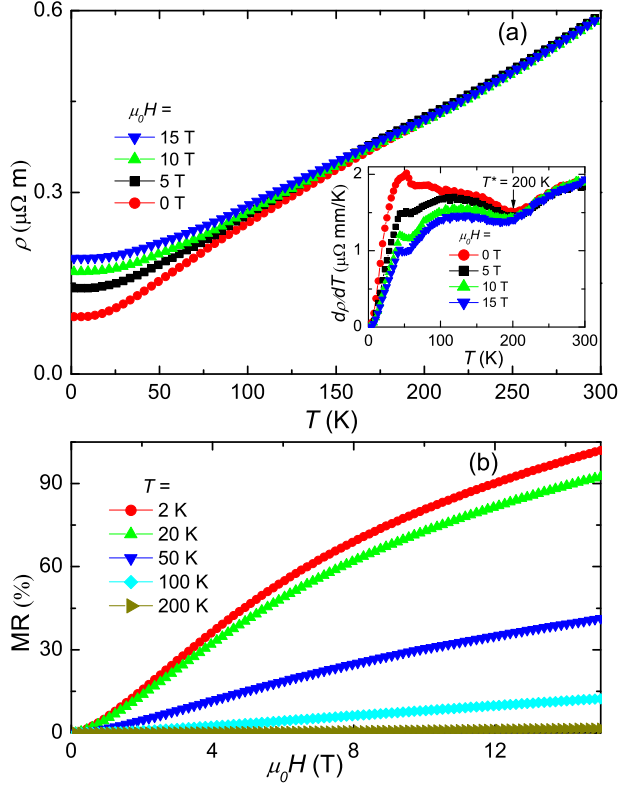


FIG. 2: **Transport properties of NbTe₄ at ambient pressure.** (a), Plots of resistivity against temperature under $\mu_0 H = 0, 5, 10,$ and 15 T. The current is along the c -axis, and the field is along the b -axis. Inset: Plots of $d\rho/dT$ versus temperature. (b), Field dependence of $MR = [\rho(H) - \rho(0)]/\rho(0)$ under various temperatures.

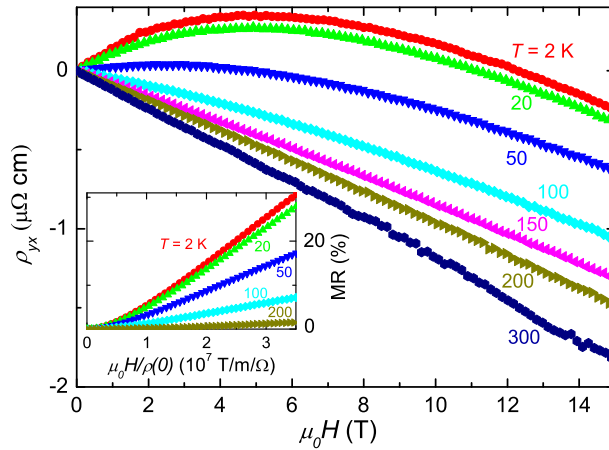


FIG. 3: **Hall resistivity and Kohler plot for NbTe₄.** Field dependence of Hall resistivity (ρ_{yx}) under various temperatures. The current is along the c -axis, and the field is along the b -axis. The inset: Kohler's rule by plotting the MR vs. $\mu_0 H / \rho(0)$ from 2 K to 200 K.

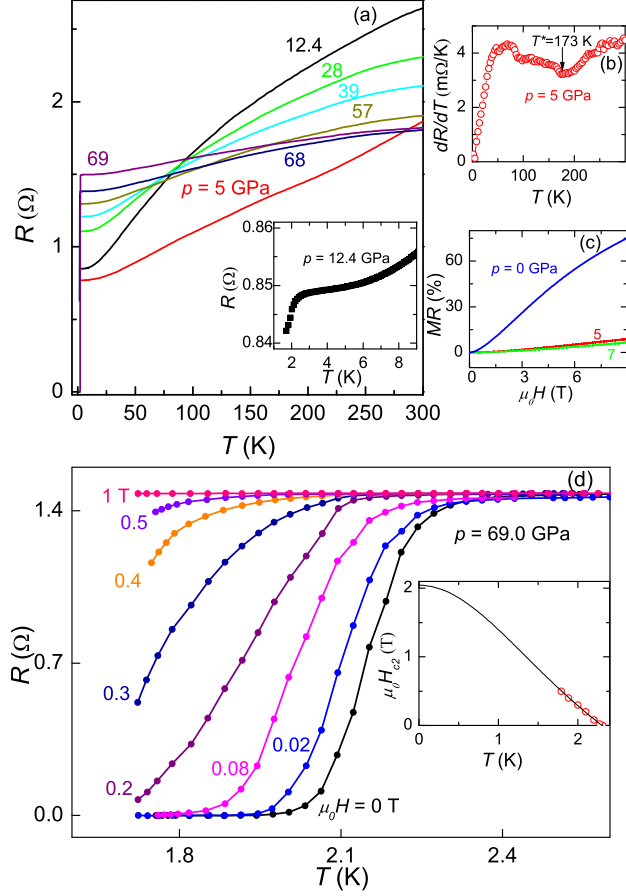


FIG. 4: **Transport properties for single crystal NbTe₄ under pressure.** (a), The plot of resistance versus temperature for the pressure ranging from 5 GPa to 69 GPa. The current is along the c -axis. The inset: The enlarged plot of resistance at low temperatures under $p = 12.4$ GPa. (b), Plots of dR/dT versus temperature under $p = 5$ GPa. (c), Field dependence of MR under $p = 0, 5$ and 7 GPa. (d), Temperature dependence of resistance for several different magnetic fields under $p = 69$ GPa. The inset displays the upper critical fields as a function of temperatures.

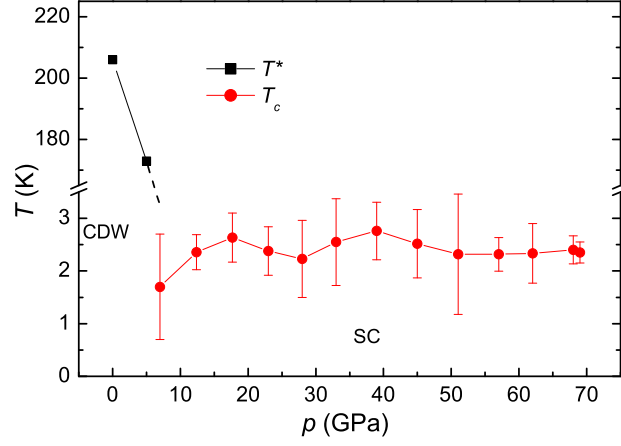


FIG. 5: **Temperature versus pressure phase diagram of NbTe_4 .** T^* and T_c denote the resistivity anomaly temperature and the superconducting transition temperature, respectively.